Relaxation of optically excited carriers in graphene

Raseong Kim,[1] Vasili Perebeinos,[2] and Phaedon Avouris[2]

[1]*Network for Computational Nanotechnology, Purdue University, West Lafayette, Indiana 47907, USA*
[2]*IBM Thomas J. Watson Research Center, Yorktown Heights, New York 10598, USA*

We explore the relaxation of photoexcited graphene by solving a transient Boltzmann transport equation with electron-phonon (e-ph) and electron-electron (e-e) scattering. Simulations show that when the excited carriers are relaxed by e-ph scattering only, a population inversion can be achieved at energies determined by the photon energy. However, e-e scattering quickly thermalizes the carrier energy distributions washing out the negative optical conductivity peaks. The relaxation rates and carrier multiplication effects are presented as a function of photon energy, graphene doping, and dielectric constant.

I. INTRODUCTION

Following the success in fabricating field-effect transistors using a single carbon atom layer,[1] graphene has been actively studied as a possible basis for electronic and optoelectronic devices.[2] Graphene's linear dispersion and zero energy gap result in unique transport and optical properties,[3–5] and new device concepts have been proposed to make use of those special features.[6] Recently, a new type of terahertz laser based on graphene has been proposed.[7–9] Analytical model calculations considering relaxation involving optical-phonon emission have shown that with sufficiently strong optical pumping, population inversion and negative ac conductivity may be achieved in the terahertz frequency range.[7,10,11] This results from the fast optical-phonon relaxation followed by an acoustic-phonon relaxation bottleneck for excited electrons and holes with energies $E_F - \hbar\omega_o \leqslant E \leqslant E_F + \hbar\omega_o$, where E_F is the Fermi level, and $\hbar\omega_o$ is the optical-phonon energy. The threshold pumping power needed to obtain population inversion depends on the carrier recombination mechanism.[7]

It has been recognized for a long time that coupling between electronic and phonon decay mechanisms can change dramatically as dimensionality of the material is reduced. The carrier multiplication due to the enhanced Coulomb scattering in zero-dimensional quantum dots[12] and one-dimensional carbon nanotubes[13] has been actively explored for potential optoelectronic applications including solar energy harvesting.[14] Previous studies on two-dimensional (2D) quantum-well systems[15] have shown that electron-electron (e-e) scattering is responsible for the fast relaxation of photoexcited carriers, and recent experiments on 2D graphene[16] also report ultrafast carrier kinetics. Unlike in bulk materials, Coulomb interactions in low-dimensional materials can also be modified by the dielectric environment, which is responsible for the screening of Coulomb interactions among carriers. Therefore, it is essential to explore the effects of Coulomb interactions and phonon scattering on carrier dynamics for the experimentally accessible carrier densities, dielectric environments, and optical excitation conditions. In this work, we simulate steady-state and time-resolved behaviors of photoexcited carriers in graphene.

II. SIMULATION METHODS

In this work, we solve a time-dependent Boltzmann transport equation (BTE) for 2D graphene with optical pumping. We consider carrier scattering and recombination-generation (RG) mechanisms including acoustic- and optical-phonon scattering,[17–19] charged impurity scattering,[20] photogeneration,[4] spontaneous optical transition,[10] and e-e scattering that includes impact ionization and Auger recombination.[21] Using the numerical solutions of the BTE, we study the influence of each scattering mechanism on the properties of optically pumped graphene, compare the results with those from previous approaches, i.e. with phonon scattering only,[7] and address the challenges involved in realizing population inversion. We solve the BTE as

$$\frac{f_{s\mathbf{k}}^{n+1} - f_{s\mathbf{k}}^n}{\Delta t} = \frac{e\mathscr{E}_x}{\hbar}\frac{\partial f_{s\mathbf{k}}^n}{\partial k_x} + \hat{C}f_{s\mathbf{k}}^n + G_{s\mathbf{k}}^n, \tag{1}$$

where $f_{s\mathbf{k}}^n$ is the distribution function at the n*th* time step for a state with 2D wave vector $\mathbf{k} = (k_x, k_y)$ in the conduction ($s = +1$) or in the valence ($s = -1$) band, e is the unit charge, $\hbar$ is the reduced Planck constant, $\mathscr{E}_x$ is the electric field along the x direction, $\hat{C}f_{s\mathbf{k}}^n$ and $G_{s\mathbf{k}}^n$ are the collision integral and the RG rates, correspondingly, and Δt is the time interval, which is 0.05–10 fs in our simulation. We treat a bulk graphene under uniform illumination, so f_s has no spatial dependence.

The collision integral treats carrier scattering as

$$\hat{C}f_{s\mathbf{k}} = \sum_{\mathbf{k}'} f_{s'\mathbf{k}'}(1 - f_{s\mathbf{k}})S_{\mathbf{k}',\mathbf{k}} - \sum_{\mathbf{k}'} f_{s\mathbf{k}}(1 - f_{s'\mathbf{k}'})S_{\mathbf{k},\mathbf{k}'},$$

where $S_{\mathbf{k},\mathbf{k}'}$ is the transition rate from $\mathbf{k}$ to $\mathbf{k}'$, and $ss' = \pm 1$ means the intra- and interband transition, respectively. For the two acoustic-phonon modes, Γ_{LA} and Γ_{TA}, the sum of the two contributions can be treated as isotropic using an averaged sound velocity υ_S as

$$S_{\mathbf{k},\mathbf{k}'} = \frac{2\pi}{\hbar}\frac{D_A^2\beta}{2A\upsilon_F\rho_m\upsilon_S}\left(N_\omega + \frac{1}{2} \mp \frac{1}{2}\right)\delta_{\mathbf{k}',\mathbf{k}\pm\boldsymbol{\beta}}$$
$$\times \delta(k' - k \mp \beta\upsilon_S/\upsilon_F),$$

where D_A is the acoustic-phonon deformation potential, $\boldsymbol{\beta}$ is the 2D phonon wave vector with magnitude β, ρ_m is the mass density, A is the area of the sample, υ_F is the Fermi velocity, N_ω is the Bose-Einstein phonon occupation number, δ is the Dirac δ function, and $\mp$ (or $\pm$) signs represent the absorption and emission of phonons. For $D_A = 7.1$ eV and $\upsilon_S = 17.3$ km/s,[19] we obtain a low-field mobility of

$\sim$190 000 cm^2 V^{-1} s^{-1} for carrier density of $\sim$10^{12} cm^{-2} as in the work of Chen et al.[3] Acoustic-phonon scattering is treated to be inelastic for a rigorous treatment of energy relaxation and broadening of distribution functions. Electron-phonon (e-ph) coupling of long-wavelengh optical-phonon modes, Γ_{LO} and Γ_{TO}, is expressed as[17,18]

$$S_{\mathbf{k},\mathbf{k}'} = \frac{2\pi}{\hbar} \frac{D_o^2}{2Av_F\rho_m\omega_o} \left(N_\omega + \frac{1}{2} \mp \frac{1}{2} \right) \delta \left(k' - k \mp \frac{\omega_o}{v_F} \right), \quad (2)$$

where $D_o = 3\sqrt{2}J_1/2 \sim 11$ eV Å^{-1} is the optical-phonon deformation potential with a coupling constant of $J_1 = 5.3$ eV Å^{-1},[19] and $\hbar\omega_o = 197$ meV. For zone-edge phonon modes, only the transverse mode K$_{TO}$ contributes to the carrier scattering, and the transition rate is given by Eq. (2) multiplied by $[1 - ss'\cos(\theta_\mathbf{k} - \theta_{\mathbf{k}'})]/2$,[17] with $D_o = 3J_1 \sim 16$ eV Å^{-1}, $\hbar\omega_o = 157$ meV, and $\theta_\mathbf{k}$ is the angle of $\mathbf{k}$.

While the charged impurity scattering[20] degrades the graphene mobility significantly due to momentum relaxation, we find that it has little effect on the optical properties (the main focus of this work) because it does not relax energy.

Coulomb scattering among electrons contributes to the RG process through impact ionization and Auger recombination,[21] and it can also thermalize distribution functions without changing the total carrier density. For Auger recombination and impact ionization, there are four processes involved: CCCV, VVCV, CVCC, and CVVV, where C and V represent the conduction and valence bands, and the second and the third letters represent the initial states of the two electrons involved, and the first and the fourth letters represent the final states of the corresponding electrons.[22] For example, the transition rate from $\mathbf{k}$ to $\mathbf{k}'$ in the conduction band due to CVCC is expressed as

$$S_{\mathbf{k},\mathbf{k}'} = \frac{2\pi}{\hbar^2 v_F} \sum_{\mathbf{k_1}} |M|^2 \delta(|\mathbf{k}'| + |\mathbf{k_1} + \mathbf{k} - \mathbf{k}'| - |\mathbf{k}| + |\mathbf{k_1}|)$$
$$\times f_{-1,\mathbf{k_1}}(1 - f_{+1,\mathbf{k_1}+\mathbf{k}-\mathbf{k}'}),$$

where $|M|^2 = |M_d|^2 + |M_e|^2 - (M_d - M_e)^2 = 2|M_d|^2 + 2|M_e|^2 - M_d^*M_e - M_dM_e^*$, and M_d and M_e are the direct and exchange matrix elements. To treat the K-K$'$ valley degeneracy, we double the $2|M_d|^2$ and $2|M_e|^2$ terms. Coulomb interactions are calculated using the random-phase approximation (RPA) in the static limit.[20] The resulting collision integral in Eq. (1) becomes four dimensional, and it can be reduced to two dimensions using the momentum- and energy-conservation conditions.[21] Processes conserving the number of electron-hole pairs, i.e., CCCC, VVVV, CCVV, and CVCV, are treated in a similar way.

$G_{s\mathbf{k}}$ in Eq. (1) includes photogeneration and spontaneous emission. The photogeneration rate is

$$G_{s\mathbf{k},opt} = \alpha \frac{\pi^2 v_F P_{opt}}{\hbar \omega_{opt}^2} (f_{s'\mathbf{k}} - f_{s\mathbf{k}}) \delta \left(k - \frac{\omega_{opt}}{2v_F} \right), \quad (3)$$

where α is the fine-structure constant, $\hbar\omega_{opt} \equiv E_{opt}$ is the incident photon energy, P_{opt} is the pumping power, and $ss' = -1$. From Eq. (3), we can show that the graphene with $f_{+1} = 0$ and $f_{-1} = 1$ has the absorbance of $\pi\alpha \sim 2.3\%$.[4] The spontaneous emission is treated using the approach of Vasko

and Ryzhii,[10] but its contribution is much smaller than those from other processes.

III. STEADY-STATE RESULTS

Using the models described in Sec. II, we numerically solve the BTE on a 2D k grid. We first simulate optically pumped graphene without considering e-e scattering, where e-ph scattering is the main mechanism for energy relaxation as in the previous approaches.[7,8] Then we introduce e-e scattering and see how the results change. We also explore the effects of E_{opt}, P_{opt}, and E_F on the properties of optically pumped graphene. All simulation results are for 300 K, zero $\mathscr{E}_x$, and no charged impurity. Photocurrent with finite $\mathscr{E}_x$ due to the transport of photoexcited carriers will be discussed elsewhere.

Figure 1 shows simulation results under steady-state low power optical pumping considering e-ph scattering only. In all following results, $f_{\pm 1}$ means $f_{\pm 1,\mathbf{k}}$ averaged over $\mathbf{k}$ with $|\mathbf{k}| = k$ and $E = \pm\hbar v_F k$. In Fig. 1(a) for $E_F = 0$ eV, f_{+1} under optical pumping dramatically deviates from equilibrium with peaks modulated by E_{opt}. For $E_{opt} = 0.6$ eV, for example, photoexcited electrons first generated at $E = 0.3$ eV pile up at $E \sim 0.1$ eV and 0.15 eV due to the emission of $\Gamma_{LO/TO}$ and K$_{TO}$ phonons. For $E_F = 0$ eV, photoexcited holes pile up symmetrically in the valence band. Due to interband optical phonon scattering, the piled-up electrons and holes recombine with holes and electrons in the opposite bands, so the carriers with $E < 0.1$ eV are depleted in Fig. 1(a). Figure 1(b) shows the optical absorbance due to interband transition, $\pi\alpha(f_{-1} - f_{+1})$, vs frequency $2|E|/h$, where h is the Planck constant. The absorbance becomes negative, i.e., population inversion is achieved, at specific frequency ranges
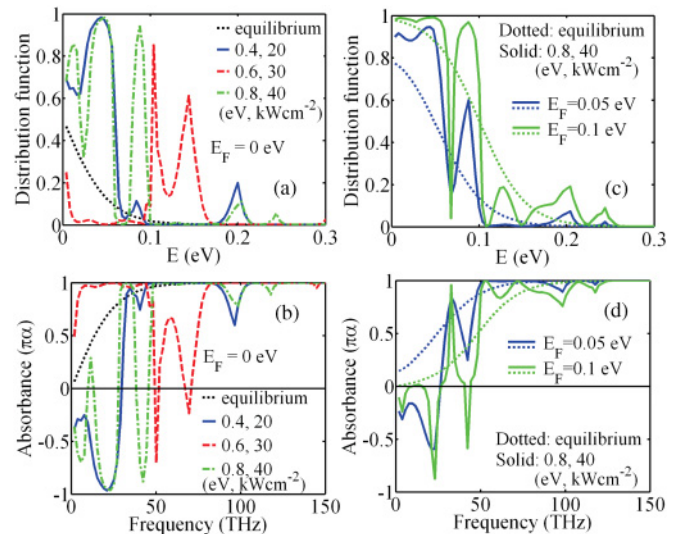

FIG. 1. (Color online) Simulation results for optically pumped graphene under steady state with e-ph scattering only. (a) f_{+1} vs E and (b) absorbance for $E_F = 0$ eV, $E_{opt} = 0.4$, 0.6, and 0.8 eV, and $P_{opt} = 20$, 30, and 40 kW cm^{-2}. (c) f_{+1} vs E and (d) absorbance for $E_F = 0.05$ and 0.1 eV, $E_{opt} = 0.8$ eV, and $P_{opt} = 40$ kW cm^{-2}. Population inversion is achieved and modulated by E_{opt}.
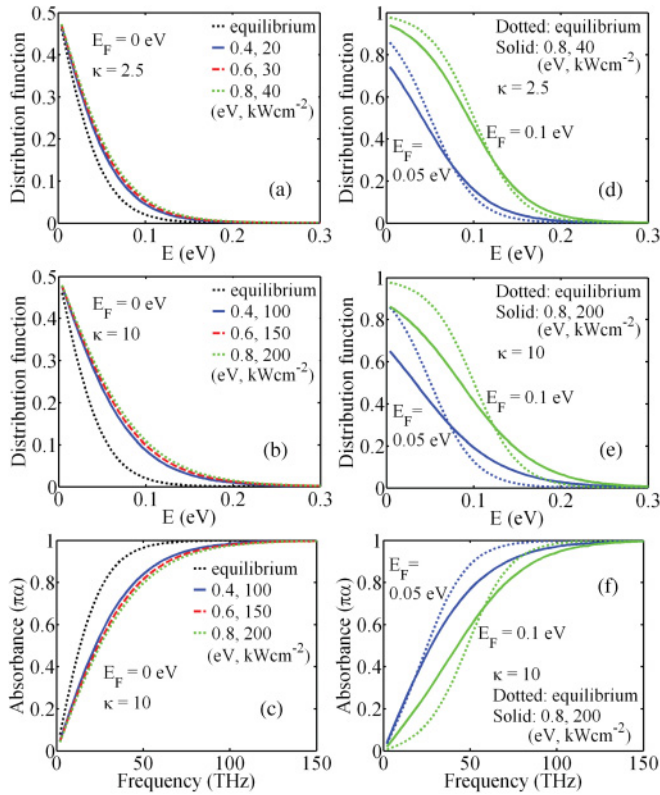
FIG. 2. (Color online) Simulation results for optically pumped graphene under steady state with e-e scattering considered. (a) f_{+1} vs E for $E_F = 0$ eV, $\kappa = 2.5$, $E_{opt} = 0.4$, 0.6, and 0.8 eV, and $P_{opt} = 20$, 30, and 40 kW cm^{-2}. (b) f_{+1} vs E and (c) absorbance with increased pumping powers and $\kappa = 10$. (d) f_{+1} vs E for $E_F = 0.05$ and 0.1 eV, $\kappa = 2.5$, $E_{opt} = 0.8$ eV, and $P_{opt} = 40$ kW cm^{-2}. (e) f_{+1} vs E and (f) absorbance with increased pumping powers and $\kappa = 10$. Distribution functions are thermalized with elevated electron temperatures, and population inversion is not achieved.

depending on E_{opt}. Simulation results for $E_F = 0.05$ and 0.1 eV are shown in Figs. 1(c) and 1(d). For finite E_F values, f_{+1} and f_{-1} are not symmetric, and the frequency and the height of the population inversion peaks depend on E_F. In general, as E_F increases, a smaller energy region becomes available for the minority carriers to experience an acoustic-phonon bottleneck, so a larger pumping power is required to invert the population.

Figure 2 shows simulation results for optically pumped graphene under steady state with e-e scattering considered. In Fig. 2(a) for $E_F = 0$ eV and dielectric constant $\kappa = 2.5$, f_{+1} with optical pumping does not deviate much from equilibrium, and there is little E_{opt}-dependence unlike the case of Fig. 1(a). We find that under photoexcitation the distribution function remains equilibrium with an elevated electronic temperature T_e determined from the Fermi-Dirac distribution. In Fig. 2(a), $T_e = 381$, 402, and 419 K for $E_{opt} = 0.4$, 0.6, and 0.8 eV, respectively. In Fig. 2(b), although we increase P_{opt} by five times and use a high $\kappa = 10$ to reduce the Coulomb interaction, the distribution functions are more broadened with higher T_e values (497, 529, and 553 K) and still far from population inversion, and the absorbance never goes below zero in Fig. 2(c). Here we should note that
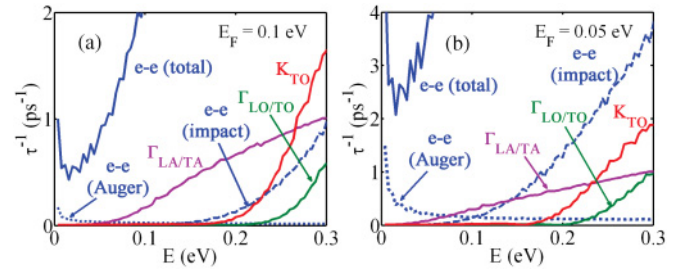

FIG. 3. (Color online) Simulation results for τ^{-1} vs E (conduction band, $\kappa = 10$) under equilibrium with (a) $E_F = 0.1$ eV and (b) $E_F = 0.05$ eV. Coulomb scattering rates are much larger than e-ph scattering rates and increase with decreasing E_F.

in RPA,[20] the Coulomb interaction does not scale as κ^{-2} as expected from the unscreened model. For $E_F = 0$ eV, for example, the RPA coincides with the unscreened model with $\kappa + e^2/(8\hbar v_F \varepsilon_0) \sim \kappa + 3.5$ where ε_0 is the vacuum permittivity, so changing κ from 2.5 to 10 results in the Coulomb interaction being reduced by about 5 times, not by 16 times. Simulation results for $E_F = 0.05$ and 0.1 eV are shown in Figs. 2(d)–2(f). In Fig. 2(d), population inversion is never achieved for $\kappa = 2.5$ and the same P_{opt} values as those in Fig. 1(c), and the distribution functions are thermalized with $T_e = 408$ and 379 K for $E_F = 0.05$ and 0.1 eV, respectively. With $\kappa = 10$ and larger pumping powers in Figs. 2(e) and 2(f), distribution functions are more broadened with elevated T_e's (536 and 494 K) instead of showing multiple peaks as in Fig. 1(c).

Therefore, e-e scattering significantly broadens the distribution functions washing out peaks due to cascade emission of optical phonons.[15] To observe this quantitatively, we calculate the carrier lifetime $\tau_{s,\mathbf{k}} = \sum_{\mathbf{k}'}(1 - f_{s'\mathbf{k}'})S_{\mathbf{k},\mathbf{k}'}$, which is the characteristic time it takes for a carrier in the state with $\mathbf{k}$ to scatter out to other states. Figure 3 shows results for τ^{-1} vs E for conduction band under equilibrium with $E_F = 0.1$ and 0.05 eV and $\kappa = 10$, where τ is the average of $\tau_{\mathbf{k}}$ for $|\mathbf{k}| = k$. The contribution from e-e scattering scales linearly with E, and it is much larger than those from e-ph scattering and increases with decreasing E_F due to reduced screening. The finite T_e corrections,[23] the finite frequency corrections,[24] and higher order contributions beyond the RPA[25] to the polarizability function are expected to modify the scattering rates, especially at low doping level, small momentum transfer q, and small κ. In experiments, electron-hole puddles are inevitable, which would reduce the influence of the finite T_e. For the large q determined by the laser energy, the finite T_e corrections are negligible. For a small q, screening can be treated more rigorously by calculating the polarization function using the self-consistent distribution function from Eq. (1). In this work, however, we explored a large range of κ, and our main conclusion that e-e scattering modifies the distribution function dramatically is not expected to change.

IV. TIME-RESOLVED CARRIER DYNAMICS

So far we have mainly discussed steady-state results, but transient responses[26] are also important in understanding carrier dynamics in graphene. In Figs. 4(a) and 4(b), we
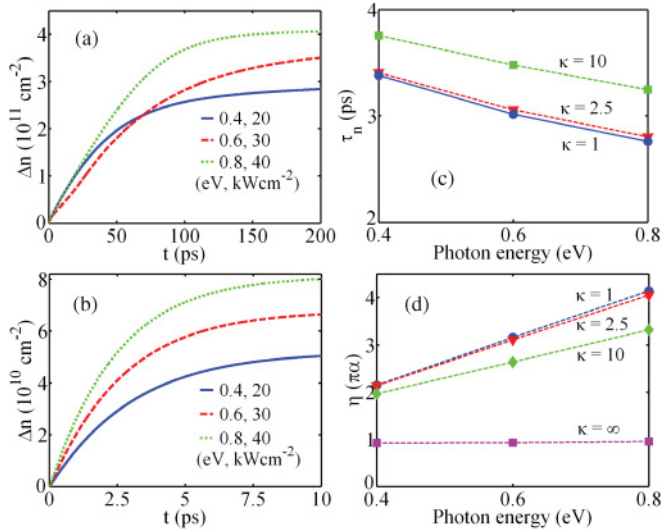
FIG. 4. (Color online) Simulation results for Δn vs t with optical pumping ($E_{opt} = 0.4$, 0.6, and 0.8 eV, $P_{opt} = 20$, 30, and 40 kW cm^{-2}) for $E_F = 0$ eV with (a) e-ph scattering only and (b) e-e scattering considered with $\kappa = 2.5$. (c) Relaxation time vs E_{opt} and (d) absorption efficiency vs E_{opt} for various κ values for the same optical pumping conditions.

compare the photocarrier density $\Delta n = n - n_0$ vs t for $E_F = 0$ eV with and without e-e scattering ($\kappa = 2.5$), where n is the total electron density, n_0 is the equilibrium electron density, and the optical pumping starts at time $t = 0$ ps. With e-e scattering, steady state is quickly achieved, and Δn, which in turn determines the photocurrent response,[2] is much smaller than with e-ph scattering only. We can fit the Δn vs t curves using $\Delta n = A_n \tau_n [1 - \exp(-t/\tau_n)]$ and extract the relaxation time τ_n and the absorption efficiency $\eta = A_n/R_{opt}$, where $R_{opt} = P_{opt}/E_{opt}$. For e-ph scattering only in Fig. 4(a), τ_n is very large (45–60 ps) and increases with E_{opt} while it is much shorter for e-e scattering ($\sim$3 ps) in Fig. 4(b). As shown in Fig. 4(c), τ_n increases with increasing κ and somewhat decreases with increasing E_{opt}. Figure 4(d) shows the η vs E_{opt} results. For $\kappa = \infty$ (i.e., e-ph scattering only), η is close to $\pi \alpha$ and independent of E_{opt}. For finite κ's, however, η is greater than $\pi \alpha$, which indicates carrier multiplication. The η increases with decreasing κ due to the increased Coulomb interaction, and it increases with increasing E_{opt} because

high-energy photocarriers have higher ability to initiate impact ionization. A recent theoretical study has reported that with pulse excitations, impact ionization leads to dramatically increased photocarrier densities.[27] However, for continuous excitation (the main focus of this work), e-e scattering leads to a lower steady-state $\Delta n = A_n \tau_n$ because Auger recombination becomes stronger and recombination due to optical-phonon emission is boosted by the broadened distribution functions, which all result in a reduced τ_n. We find that T_e follows a similar time evolution as Δn, and the steady-state T_e under optical pumping depends on E_{opt}, P_{opt}, and κ as shown in Fig. 2. We also find that the decay time constant, after the optical pumping is switched off, is slightly different than the rise time constant due to the difference in the scattering rate determined by the distribution function in the photoexcited state.

V. SUMMARY

In summary, we numerically solved a time-dependent BTE for bulk graphene considering photogeneration and relevant carrier scattering and RG mechanisms to explore properties of optically pumped graphene and possibilities to achieve population inversion. Simulation results showed that when carrier energies are relaxed by e-ph scattering only, it is possible to achieve population inversion at frequencies controlled by incident photon energy and graphene Fermi level. A more realistic model considering Coulomb scattering, however, showed that distribution functions are significantly broadened, and it becomes hard to achieve population inversion even with much higher pumping power. The results stress the importance of e-e scattering in carrier dynamics in graphene and suggest that the Coulomb interaction among carriers must be significantly suppressed, such as by band-gap opening in bilayer graphene, to realize graphene-based terahertz lasers. However, e-e scattering leads to significant carrier multiplication.

ACKNOWLEDGMENTS

[1]K. S. Novoselov, A. K. Geim, S. V. Morozov, D. Jiang, Y. Zhang, S. V. Dubonos, I. V. Grigorieva, and A. A. Firsov, Science **306**, 666 (2004).

[2]P. Avouris, Nano Lett. **10**, 4285 (2010).

[3]J.-H. Chen, C. Jang, S. Xiao, M. Ishigami, and M. S. Fuhrer, Nat. Nanotechnol. **3**, 206 (2008).

[4]R. R. Nair, P. Blake, A. N. Grigorenko, K. S. Novoselov, T. J. Booth, T. Stauber, N. M. R. Peres, and A. K. Geim, Science **320**, 1308 (2008).

[5]K. F. Mak, M. Y. Sfeir, Y. Wu, C. H. Lui, J. A. Misewich, and T. F. Heinz, Phys. Rev. Lett. **101**, 196405 (2008).

[6]M. I. Katsnelson, K. S. Novoselov, and A. K. Geim, Nat. Phys. **2**, 620 (2006); V. V. Cheianov, V. Fal'ko, and B. L. Altshuler, Science **315**, 1252 (2007).

[7]V. Ryzhii, M. Ryzhii, and T. Otsuji, J. Appl. Phys. **101**, 083114 (2007).

[8]V. Ryzhii, M. Ryzhii, A. Satou, T. Otsuji, A. A. Dubinov, and V. Y. Aleshkin, J. Appl. Phys. **106**, 084507 (2009).

[9]H. Karasawa, T. Komori, T. Watanabe, A. Satou, H. Fukidome, M. Suemitsu, V. Ryzhii, and T. Otsuji, J. Infrared Milli. Terahz. Waves **32**, 655 (2011).

[10]F. T. Vasko and V. Ryzhii, Phys. Rev. B **77**, 195433 (2008).

[11]F. T. Vasko, Phys. Rev. B **82**, 245422 (2010).

[12]A. J. Nozik, Physica E **14**, 115 (2002).

[13]J. Chen, V. Perebeinos, M. Freitag, J. Tsang, Q. Fu, J. Liu, and P. Avouris, Science **310**, 1171 (2005); V. Perebeinos and P. Avouris, Phys. Rev. B **74**, 121410 (2006).

[14]R. D. Schaller and V. I. Klimov, Phys. Rev. Lett. **92**, 186601 (2004); R. D. Schaller, M. Sykora, J. M. Pietryga, and V. I. Klimov, Nano Lett. **6**, 424 (2006); N. M. Gabor, Z. Zhong, K. Bosnick, J. Park, and P. L. McEuen, Science **325**, 1367 (2009).

[15]S. M. Goodnick and P. Lugli, Phys. Rev. B **37**, 2578 (1988).

[16]R. W. Newson, J. Dean, B. Schmidt, and H. M. van Driel, Opt. Express **17**, 2326 (2009); H. Choi, F. Borondics, D. A. Siegel, S. Y. Zhou, M. C. Martin, A. Lanzara, and R. A. Kaindl, Appl. Phys. Lett. **94**, 172102 (2009).

[17]M. Lazzeri, S. Piscanec, F. Mauri, A. C. Ferrari, and J. Robertson, Phys. Rev. Lett. **95**, 236802 (2005).

[18]T. Ando, J. Phys. Soc. Jpn. **75**, 124701 (2006).

[19]V. Perebeinos and P. Avouris, Phys. Rev. B **81**, 195442 (2010).

[20]E. H. Hwang and S. Das Sarma, Phys. Rev. B **77**, 195412 (2008).

[21]F. Rana, Phys. Rev. B **76**, 155431 (2007).

[22]P. T. Landsberg, *Recombination in Semiconductors* (Cambridge University Press, Cambridge, UK, 1991).

[23]E. H. Hwang and S. Das Sarma, Phys. Rev. B **79**, 165404 (2009).

[24]M. Schütt, P. M. Ostrovsky, I. V. Gornyi, and A. D. Mirlin, Phys. Rev. B **83**, 155441 (2011).

[25]V. N. Kotov, B. Uchoa, and A. H. C. Neto, Phys. Rev B **78**, 035119 (2008).

[26]T. Hertel and G. Moos, Phys. Rev. Lett. **84**, 5002 (2000).

[27]T. Winzer, A. Knorr, and E. Malic, Nano Lett. **10**, 4839 (2010).